Separating Oil-Water Nanoemulsions using Flux-Enhanced Hierarchical Membranes

Citation: Solomon, Brian R., Md. Nasim Hyder, and Kripa K. Varanasi. "Separating Oil-Water Nanoemulsions Using Flux-Enhanced Hierarchical Membranes." Sci. Rep. 4 (July 1, 2014).

As Published: http://dx.doi.org/10.1038/srep05504

Publisher: Nature Publishing Group

Persistent URL: http://hdl.handle.net/1721.1/89465

Version: Final published version: final published article, as it appeared in a journal, conference proceedings, or other formally published context

SCIENTIFIC REPORTS

OPEN

SUBJECT AREAS:
MECHANICAL ENGINEERING
CHEMICAL ENGINEERING

Received
19 February 2014

Accepted
6 June 2014

Published
1 July 2014

Correspondence and requests for materials should be addressed to K.K.V. (varanasi@mit.edu)

Separating Oil-Water Nanoemulsions using Flux-Enhanced Hierarchical Membranes

Brian R. Solomon, Md. Nasim Hyder & Kripa K. Varanasi

Department of Mechanical Engineering, Massachusetts Institute of Technology, Cambridge MA 02139.

Membranes that separate oil-water mixtures based on contrasting wetting properties have recently received significant attention. Separation of nanoemulsions, i.e. oil-water mixtures containing sub-micron droplets, still remains a key challenge. Tradeoffs between geometric constraints, high breakthrough pressure for selectivity, high flux, and mechanical durability make it challenging to design effective membranes. In this paper, we fabricate a hierarchical membrane by the phase inversion process that consists of a nanoporous separation skin layer supported by an integrated microporous layer. We demonstrate the separation of water-in-oil emulsions well below 1 μm in size. In addition, we tune the parameters of the hierarchical membrane fabrication to control the skin layer thickness and increase the total flux by a factor of four. These simple yet robust hierarchical membranes with engineered wetting characteristics show promise for large-scale, efficient separation systems.

In recent years, growing environmental concerns have fueled the need for efficient separation of oil-water mixtures[1]. Oil spills, as highlighted by the Deepwater Horizon spills, have lasting detrimental ecological effects[2,3]. The threat is recurring and persistent; every year over 20,000 oil spills are reported to the U.S. government[4]. Aside from such disasters, fats, oils, and grease are classified as hazardous waste and their removal is subject to increasingly more stringent governmental regulation[5,6].

A variety of techniques have been implemented in industry, including gravity separation, skimming and dissolved air flotation[7]. More recently, new techniques incorporating aerogels[8,9], magnetic materials[10–12], and fluorosurfactant polymers[13] have been introduced. Though promising, these approaches are ineffective for separation of small-scale emulsions, especially for those with droplets below a micron in size[7,14–16].

Membranes which function primarily on the principle of size exclusion offer cost-effective separation for filtration of solid particles such as protein aggregates and macromolecules[17–19]. However, in the case of emulsified liquids, dispersed droplets can deform and squeeze through pores that are smaller than the emulsified droplet size[20]. To prevent droplets of one phase from squeezing through a membrane, the surface energy of the membrane must be controlled. In recent years, developments in the field of surface wettability have enabled new membrane technologies for the separation of oil-water mixtures. Membranes with contrasting wettability have been shown to selectively filter one phase depending on whether they are hydrophilic/oleophobic or hydrophobic/oleophilic. Most of these studies have been performed with stratified mixtures[21–27], while studies on emulsions have been relatively sparse[28–32]. Furthermore, separation of emulsions consisting of droplets below a micron in size (nanoemulsions) remains a significant challenge[29,33].

For a straight-pore membrane, complete separation of nanoemulsions requires pores smaller than the smallest droplet size. For a given applied pressure, smaller pores lead to a lower flow rate. Decreasing the thickness of the membrane can circumvent this, but extremely thin membranes lack mechanical integrity. In addition, increasing the applied pressure can increase the flow rate, but the maximum pressure must not exceed the breakthrough pressure. Hence, there is a need for new membrane architectures that can achieve both high fluxes and high selectivity while maintaining mechanical durability.

In this paper, we develop a hierarchical membrane fabricated by the phase inversion process[34,35] that consists of a nanoporous separation layer supported by an integrated microporous layer and describe a methodology based on wetting thermodynamics for the separation of nanoemulsions. We consider the implications of both the geometry and the chemical properties of the membrane. The membrane can separate emulsified droplets well below 1 μm in size. By tuning the thickness of the nanoporous separation layer, we show that the flux can be increased. The design displays potential for commercial viability due to its manufacturability and scalability while

achieving high flow rates. To begin, we present the wetting thermodynamics needed for understanding the membrane's operation.

Results

Wetting Thermodynamics and Breakthrough Pressure. Consider an emulsion in which the continuous phase is oil and the droplet phase is water as shown in Figure 1a–c. By considering the relative interfacial energies and spreading coefficients, we have shown previously[36] that for oil to selectively impregnate a texture it is required that.

$$\theta_{os(w)} < \theta_c < \theta_{ws(o)} \tag{1}$$

where $\theta_{os(w)}$ is the contact angle of oil (subscript "o") on the solid (subscript "s") in the presence of water (subscript "w"), $\theta_{ws(o)}$ is the contact angle of water on the smooth solid in the presence of oil, and θ_c is the critical impregnation angle given by $\theta_c = \cos^{-1}[(1-\phi)/(r-\phi)]$[37]. Here r is the roughness factor and ϕ the solid fraction. Note this bounds the critical angle as $0^\circ < \theta_c \leq 90^\circ$. In the particular situation when $\theta_{os(w)} = 0^\circ$, oil will spread preferentially over the surface beneath the water droplets, causing water droplets to float on the water droplets to float on the surface of the membrane while oil permeates the membrane. In the case of a porous membrane without interconnecting pores the critical contact angle becomes 90° [37].

A limiting factor in separation arises from the breakthrough pressure[38,39]. The breakthrough pressure is the minimum pressure at which a water droplet will push through the pore despite otherwise unfavorable wetting characteristics and geometrical constraints. Provided the droplet radius is larger than the pore radius r_p, a droplet will permeate the membrane at pressures exceeding the breakthrough pressure P_B which follows from the Young-Laplace equation:

$$P_B = \frac{2\gamma_{wo}\cos\theta_{adv,ws(o)}}{r_p} \tag{2}$$

where γ_{wo} is the water-oil interfacial tension and $\theta_{adv,ws(o)}$ is the advancing angle of water on smooth solid in the presence of oil. The pressure drop across the membrane ΔP must be kept below P_B. Accordingly, this upper bound on the operating pressure limits the maximum operating flow rate.

To demonstrate the concept of the breakthrough pressure, we tested a hydrophobic/oleophilic membrane under different operating pressures. A polycarbonate track-etch membrane (EMD

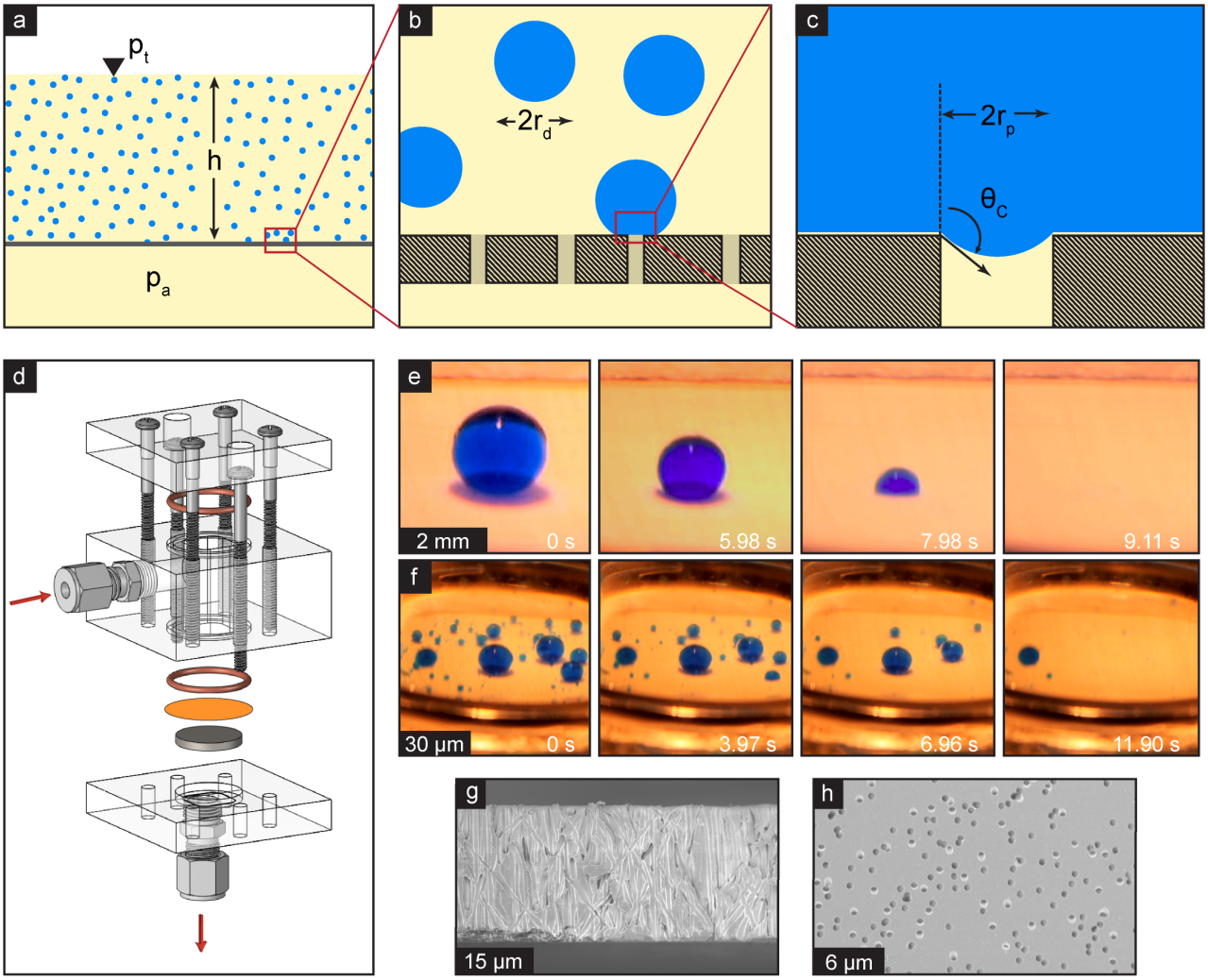

Figure 1 | Demonstration of breakthrough pressure for polycarbonate membrane. (a) Schematic of a water-in-oil emulsion being filtered through a membrane showing (b) water droplets near the membrane pores. (c) Close-up diagram of a rejected droplet on the surface of the membrane. (d) Schematic of pressurized flow cell device used for experiments. (e) Sequential images showing a 2 mm diameter water droplet breaking through a 600 nm OTS coated polycarbonate membrane after the transmembrane pressure had exceeded 170 kPa. (f) Images showing droplets of many sizes breaking through a 600 nm OTS coated polycarbonate membrane after the transmembrane pressure had exceeded 170 kPa. The remaining droplet in the last frame is actually stuck to the side of the filtration cell. (g) SEM images of an OTS coated 600 nm polycarbonate membrane showing its morphology and (h) top surface.

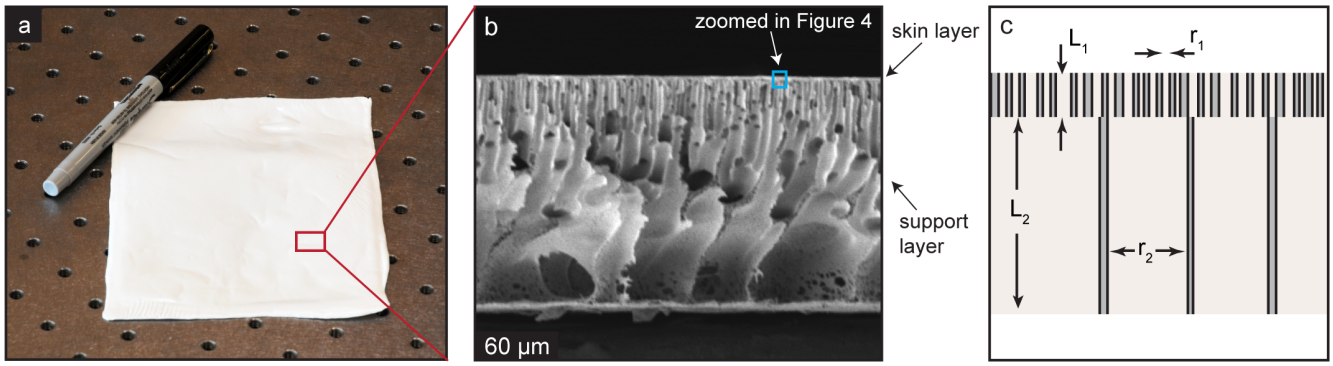

Figure 2 | Image and schematic of hierarchical membrane. (a) Photos of a cast PSf membrane. (b) SEM of the cross-section of a PSf membrane showing the hierarchical geometry featuring a skin layer. (c) Idealized schematic of a hierarchical membrane showing a skin layer with small pores and a support layer with larger pores (not to scale). The denoted region with the skin layer in (b) is shown in Figure 4 for two separate fabrications. Additional SEM images are provided in Figure S3.

Millipore) with pores of 600 nm in diameter was coated with octadecyltrichlorosilane (OTS, Sigma-Aldrich). OTS increases the oleophilicity of the membrane while also increasing its hydrophobicity. As shown in Figure 1d–f, a custom-built acrylic filtration cell was filled with n-hexadecane and dyed water droplets were placed on the surface of the polycarbonate membrane. On a flat OTS-coated substrate, measurements of $\theta_{os(w)}$ and $\theta_{ws(o)}$ indicate that hexadecane with Span 80 completely spreads in the presence of water and water forms nearly spherical droplets in the presence of hexadecane ($\theta_{os(w)} \sim 0^\circ$ and $\theta_{ws(o)} \sim 180^\circ$). These contact angles indicate that there is a thin film of oil under the water droplets as shown in Figure 1c. The chamber was then slowly pressurized and the oil began flowing through the membrane while the water droplets remained on the surface. When the pressure drop was raised above the breakthrough pressure of 170 kPa water droplets began to penetrate the membrane. Figure 1e demonstrates this effect for one large droplet of diameter 1 mm, and Figure 1f repeats the process with a distribution of droplet sizes.

Hierarchical Membranes. A caveat of polycarbonate and similar membranes is in their straight-pore geometry. The challenges of such architecture become clear when looking at Darcy's law describing the volumetric flow Q of a fluid of viscosity μ through a membrane of area A, permeability k, thickness L, and pores of radius r subject to a transmembrane pressure ΔP.

$$Q = \frac{-kA}{\mu}\frac{\Delta P}{L} \sim r^4 \tag{3}$$

The thickness of the membrane must be sufficient to render the membrane mechanically robust. As evident, while small pores achieve higher breakthrough pressures, the flow rate for such geometries decreases rapidly. The maximum flow rate while still rejecting water droplets is found by setting the transmembrane pressure to the breakthrough pressure and can be expressed in the following relation.

$$Q_{\max} = \frac{\rho_p A \gamma_{wo} \pi \cos\theta_{adv,ws(o)}}{4\mu}\frac{r^3}{L} \tag{4}$$

Here ρ_p is the number pore density, γ_{wo} is the interfacial tension between water and oil, and $\theta_{adv,ws(o)}$ is the advancing contact angle of a water droplet on the membrane surface in the presence of oil. This equation explicitly shows how flow rate is increasingly limited for decreasing pore sizes. For track-etch membranes, the number pore density is the same regardless of the size of the pores and limits the achievable flow rates. Figure S1 demonstrates experimentally the trade-off between flow resistivity and breakthrough pressure of a straight-pore membrane know as Darcy's law. As the pore size decreases and the breakthrough pressure increases, so does the resistivity. In addition, the track-etch membranes process is not scalable to large area membranes that are needed to filter the large volumes of wastewater generated at recovery and refining sites[40,41].

We demonstrate a different approach by developing hierarchical membranes consisting of a nanoporous separation layer that is integrated with a microporous support layer. This geometry offers the potential to overcome flow rate limitations. Consider an ideal hierarchical structure with two layers (Figure 2c). The thin nanoporous layer enhances selectivity while the thick microporous layer provides mechanical stability. As the nanoporous layer becomes thinner, a higher flow rate can be achieved for a set membrane thickness and minimum pore size.

$$Q_{\max} = \frac{\rho_p A \gamma_{wo} \pi \cos\theta_{adv,ws(o)}}{4\mu r_1}\left(\frac{1}{\frac{L_1}{r_1^4} + \frac{L_2}{r_2^4}}\right) \tag{5}$$

Here ρ_p is the pore density and A the area of the membrane. The subscripts denote the skin layer (1) and support layer (2) and the variables L and r are the thickness and pore size of the respective layers.

We achieve this structure by employing the non-solvent induced phase inversion technique[35]. Mixtures of polysulfone (PSf) and polyvinylpyrrolidone (PVP) were dissolved in dimethylacetamide (DMAc). Upon curing the PSf in water, the PVP macromolecules migrate to the surface and leave behind a porous matrix. Figure 2a–b shows a sheet of the cast membrane and an SEM image of the cross-section of the membrane is shown. The structure features a thin skin layer with nanopores (~30–80 nm) and a thicker layer with micropores (~10–20 μm). The morphology and chemistry of the skin-layer for our PSf membrane is critical to the performance of the membrane since it remains in contact with the feed emulsion during the pressurized separation. Although this type of this type of membrane has been used for ultrafiltration, they have sparsely been explored for separation of oil/water nanoemulsions.

To demonstrate the effectiveness of these membranes, a cast sheet was cut into 25 mm filters and treated with OTS. A feed emulsion comprising 3 wt% water and 97 wt% n-hexadecane was used for the experiments. The oil phase contained 1 wt% Span 80 to stabilize emulsified droplets. In the absence of surfactant, the emulsion spontaneously coalesces to a noticeable degree. The surfactant was employed to prevent any coalescence that would otherwise occur over the course of an experiment.

The filtration cell was run at a pressure drop of 275 kPa. The feed emulsion was filtered and the permeate collected. The cloudy feed emulsion, imaged using optical microscopy, consisted of water droplets with a mean diameter of 1.5 μm as shown in Figure 3b. In addition to microscopy, dynamic light scattering (DLS) was used to determine the size distribution of smaller droplets. DLS data show the presence of droplets around 200 nm in the feed as indicated by the middle peak in Figure 3f.

Passing the feed emulsion through the hierarchical membrane at a pressure drop of 275 kPa yields a visually clear permeate and optical microscopy shows no evidence of droplets that were otherwise evident in the feed emulsion (Figure 3d). This finding was supported by the DLS measurement where the 200 nm droplets are non-existent in the permeate data. Instead, only a species with diameter around 10 nm is present. A peak falling in the same size range was also visible in a solution of n-hexadecane containing only 1 wt% Span 80 without any water suggesting that the species is not water but due to instrumentation error, a micellar formation of Span 80, or other impurities.

In addition, differential scanning calorimetry (DSC) was used to probe the water content in the permeate samples by monitoring the heat flow into a sample[42]. Samples were frozen to −20°C and then thawed at a rate of 2.4°C s^{-1}. Since the crystalized water phase melts around 0°C and hexadecane around 18°C, the disparity in melting points of water and oil allow the data to resolve into separate peaks corresponding to the water and hexadecane phases. The feed emulsions show a noticeable peak at 0°C indicating the presence of water. This peak is not present in the permeate sample indicating the filtration process has removed water beyond any discernable level. The recovery of pure hexadecane from an emulsion containing droplets of water below a micron in size is the first direct demonstration to our knowledge of filtering nanoemulsions based on wettability.

Tuning the skin layer thickness. For the first time, we were able to employ an additional additive to the phase inversion process to control the resulting thickness of the skin layer. While PVP and PEG have been used individually to control pore size, we employ a combination to tune the thickness. In this study, the thickness of the skin layer was varied by a factor of four by using additives during the membrane's fabrication. The skin layer is created when the PVP hydrophilic polymers diffuse out of the bulk DMAc solution and into the surrounding water. In doing so, they leave behind small pores. We hypothesized that increasing the hydrophilicity of such polymers would increase their diffusion rate and thus result in a thinner skin layer.

PVP is hydrophilic due to it carboxyl groups[43]. Polymers such as polyethylene glycol (PEG) are more hydrophilic than PVP owing to their hydroxyl groups, and thus will diffuse more quickly out of the bulk solution when immersed. In a typical process, 7 g of PSf and 3 g of PVP/PEG were dissolved in 40 mL of DMAc. The ratio of polymer (PSf) to pore former (PVP/PEG) was kept constant, but the ratio of PVP to PEG was varied. PEG is a polymer chain available in varying sizes. In order to encourage more rapid diffusion during the phase inversion, relatively small sized PEG molecules with a weight-averaged molecular weight of 4,000 g/mol was used. For comparison, the weight-averaged molecular weight of the PVP used was 40,000 g/mol.

The resulting membranes had varying skin layer thicknesses ranging from 270 nm to 1.2 μm. Two membranes with skin layer thicknesses of 270 nm and 1.2 μm were chosen for a permeability study. Both membranes had pores in the skin layer ranging from 30 to 80 nm. Their relative dimensions are highlighted in the cross-section views of Figure 4. The fluxes of pure hexadecane through these two fabricated PSf membranes were measured to demonstrate the capacity. The flux through the membrane with the 270 nm skin layer measured 3.75 ± 0.56 m h^{-1} MPa^{-1}. The flux through the membrane with the 1.2 μm skin layer measured 0.935 ± 0.006 m h^{-1} MPa^{-1}. As predicted, reducing the skin layer thickness by a factor of four increases the flow rate through the membrane by over a factor of four. By further tuning the fabrication parameters, the skin layer can be thinned further to achieve even better flow rates. Additionally, the flux depends on the viscosity of the permeating liquid; lower viscosity fluids result in higher fluxes[30].

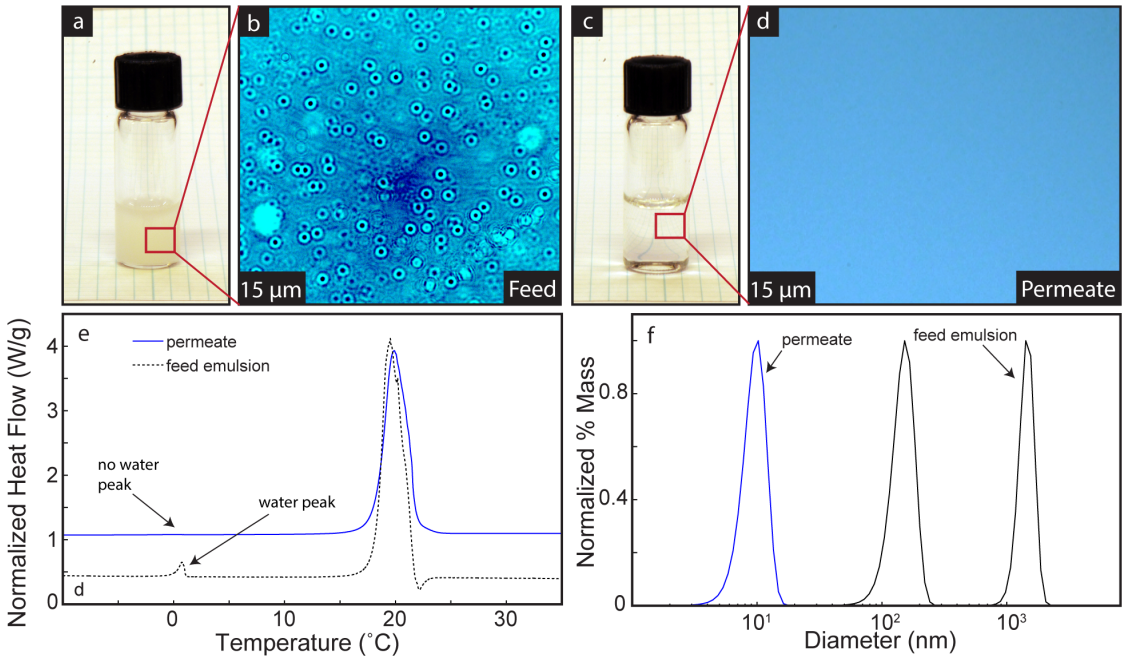

Figure 3 | Separation of an emulsion by PSf membrane. Photographs and microscopic images of a 3 wt% w/o emulsion stabilized by Span 80 (a), (b) before filtration and (c), (d) filtered through the hierarchical PSf membrane coated with OTS at a transmembrane pressure below the breakthrough pressure. (e) DSC data for the emulsion before filtration (black) and filtered through the hierarchical PSf membrane coated with OTS (blue). (f) Distribution of droplets in the feed emulsion (black) and permeate (blue). The two peaks for the feed emulsion represent measurements from DLS (centered around 10^2 nm) and microscopic image analysis (centered around 1 μm).

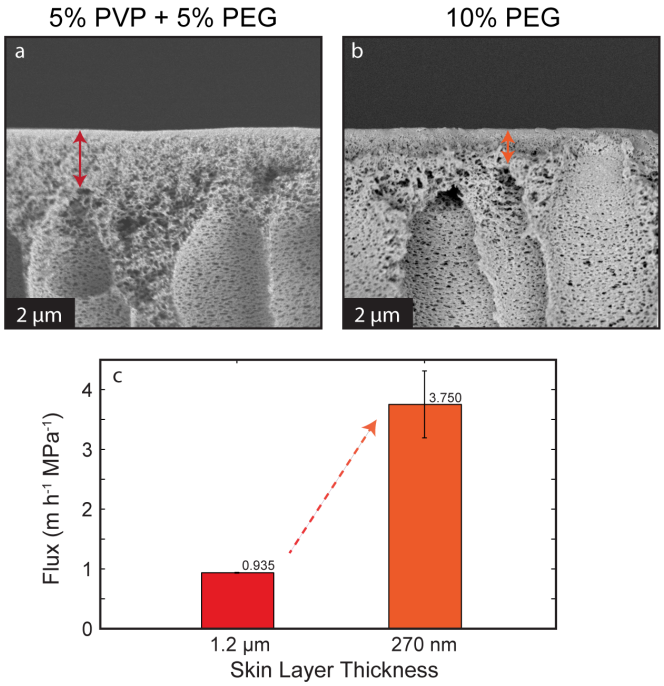

Figure 4 | Tuning skin layer thickness to maximize flux. Zoomed in SEM images of two fabricated PSf membranes show the effect of pore forming agents in the phase inversion process to create (a) a relatively thick skin layer and (b) a relatively thick skin layer. (c) Bar plot showing improved flux by reducing skin layer thickness with 90% CI error bars.

Discussion

To date, many membrane technologies for emulsion separation have been presented in the literature but have not been well characterized based on the size of droplets they separate. We demonstrate a crucial tradeoff that arises in membrane design: permeate selectivity versus permeate flux. Small pores increase selectivity but decrease flow, whereas large pores are less selective but maintain high flow rates. The methodologies presented here apply to such membranes provided they have sufficiently small pores. The presented hierarchical membrane based on the phase inversion process demonstrates the merging of these two regimes; a thin nanoporous layer maintains high selectivity, while a thick microporous layer yields high flow rates and mechanical stability.

The system demonstrated separates emulsified water droplets well below 1 µm in size dispersed in oil. While the system separated was of the water-in-oil type, the same principles of surface wettability extend to oil-in-water emulsions; a hydrophilic/oleophobic membrane may be used to separate oil-in-water emulsions. Such materials have been demonstrated recently to preferentially pass water and oil in simple mixtures[26,28,32,44].

We demonstrated that the thickness of the nanoporous layer can be controlled through the casting process, and that the thickness of this layer determines the flow resistance. By varying parameters of the casting process the flux through such membranes was improved by over a factor of four. Further work is needed to fabricate even thinner skin layers. Since these skin layers are integrated into a microporous support layer, they are more mechanically robust then their through-pore counterparts and can be fabricated much thinner.

Such work lays the groundwork for designing efficient emulsion separating processes and their cost-effective implementation. We envision this design methodology will extend beyond the separation of oil and water mixtures to realize separation of pharmaceutical emulsions, design of deployable separation devices, and control over phases in microfluidic devices.

Methods

Surface modification. Mesh samples were coated by submersing in a solution containing 0.5 mL of octadecyltrichlorosilane (OTS, Sigma-Aldrich) dissolved in 150 mL of toluene. After sonicating for two minutes in this solution, 650 µL of water was added. After sonicating for an addition two minutes, the samples were removed and sonicated in acetone to remove residual OTS. For polymeric samples, the coating solution was 500 µL of OTS in 100 mL of hexadecane. A similar procedure was carried out, but residual OTS was removed using excess hexadecane rather than acetone.

Membrane fabrication. A typical fabrication process uses 7 g PSf and 3 g polyvinylpyrrolidone (PVP) in 40 mL dimethylacetamide (DMAc) at 80OC. The solution is left at 50°C for 12 hours in order for air bubbles to be released. A thin layer (on the order of 300 µm) of the solution is casted on a glass plate and then immersed into water at room temperature to undergo coagulation. The membrane is rinsed with tap water for 24 hours, followed by immersion in a glycerol–water solution (volume ratio of 1 : 1) for another 24 hours before being dried at ambient conditions. To vary the skin layer thickness, 7 g of PSf was mixed with 3 g of mixtures of PVP and PEG of varying ratios.

Instrumentation and characterization. Scanning electron microscopy (SEM) images were obtained on a field-emission scanning electron microscope (JEOL 6700F, USA) at an operating voltage of 2.5 kV. The samples were coated with a 5 nm gold/palladium layer for imaging. Differential Scanning Calorimetry was carried out on a TA Instruments Discovery DSC. Dynamic Light Scattering was carried out on DynaPro NanoStar (Wyatt Technology Corporation, Santa Barbara, CA). Contact angles were measured on an OTS coated silicon surface in the presence of air using a Ramé-Hart Model 500 Advanced Goniometer.

1. Shannon, M. A. *et al.* Science and technology for water purification in the coming decades. *Nature* **452**, 301–310 (2008).
2. Schrope, M. Oil spill: Deep wounds. *Nat. News* **472**, 152–154 (2011).
3. Barron, M. G. Ecological impacts of the deepwater horizon oil spill: implications for immunotoxicity. *Toxicol. Pathol.* **40**, 315–320 (2012).
4. Jackson, L. Testimony of Lisa P. Jackson, Administrator of the U.S. Environmental Protection Agency. *Senate Comm. Environ. Public Works* (2010). at <http://www.epw.senate.gov/public/index.cfm?FuseAction=Files.View&FileStore_id=7185ac9b-889f-40ea-9925-14f346518a63> *Date of access:04/30/2014*.
5. Reilly, W., O'Farrell, T. & Rubin, M. Development Document for 1991 Proposed Effluent Limitation Guidelines and New Source Performance Standards for the Offshore Subcategory of the Oil and Gas Extraction Point Source Category. *US Environ. Prot. Agency* (1991).
6. Group, W. B. Pollution prevention and abatement handbook. *Oil Gas Dev. Onshore Guidel.* (1998).
7. Coca-Prados, J. & Gutiérrez-Cervelló, G. *Water Purification and Management.* (Springer, 2011).
8. Reynolds, J. G., Coronado, P. R. & Hrubesh, L. W. Hydrophobic aerogels for oil-spill clean up – synthesis and characterization. *J. Non-Cryst. Solids* **292**, 127–137 (2001).
9. Venkateswara Rao, A., Hegde, N. D. & Hirashima, H. Absorption and desorption of organic liquids in elastic superhydrophobic silica aerogels. *J. Colloid Interface Sci.* **305**, 124–132 (January 1).
10. Chen, N. & Pan, Q. Versatile Fabrication of Ultralight Magnetic Foams and Application for Oil-Water Separation. *ACS Nano* (2013).
11. Calcagnile, P. *et al.* Magnetically Driven Floating Foams for the Removal of Oil Contaminants from Water. *ACS Nano* **6**, 5413–5419 (2012).
12. Pavía-Sanders, A. *et al.* Robust Magnetic/Polymer Hybrid Nanoparticles Designed for Crude Oil Entrapment and Recovery in Aqueous Environments. *ACS Nano* (2013). doi:10.1021/nn401541e.
13. Howarter, J. A., Genson, K. L. & Youngblood, J. P. Wetting Behavior of Oleophobic Polymer Coatings Synthesized from Fluorosurfactant-Macromers. *ACS Appl. Mater. Interfaces* **3**, 2022–2030 (2011).
14. Cheryan, M. & Rajagopalan, N. Membrane processing of oily streams. Wastewater treatment and waste reduction. *J. Membr. Sci.* **151**, 13–28 (1998).
15. Kota, A. K. & Tuteja, A. High-efficiency, ultrafast separation of emulsified oil-water mixtures. *NPG Asia Mater* **5**, e58 (2013).
16. Li, K. *et al.* Structured cone arrays for continuous and effective collection of micron-sized oil droplets from water. *Nat. Commun.* **4** (2013).
17. Nunes, S. P., Sforça, M. L. & Peinemann, K.-V. Dense Hydrophilic Composite Membranes for Ultrafiltration. *J. Membr. Sci.* **106**, 49–56 (1995).
18. Hancock, L. F., Fagan, S. M. & Ziolo, M. S. Hydrophilic, semipermeable membranes fabricated with poly(ethylene oxide)–polysulfone block copolymer. *Biomaterials* **21**, 725–733 (2000).
19. Ochoa, N. A., Masuelli, M. & Marchese, J. Effect of hydrophilicity on fouling of an emulsified oil wastewater with PVDF/PMMA membranes. *J. Membr. Sci.* **226**, 203–211 (2003).
20. Cobos, S., Carvalho, M. S. & Alvarado, V. Flow of oil–water emulsions through a constricted capillary. *Int. J. Multiph. Flow* **35**, 507–515 (2009).
21. Feng, L. *et al.* A Super-Hydrophobic and Super-Oleophilic Coating Mesh Film for the Separation of Oil and Water. *Angew. Chem. Int. Ed.* **43**, 2012–2014 (2004).

22. Yuan, J. *et al.* Superwetting nanowire membranes for selective absorption. *Nat Nano* **3**, 332–336 (2008).
23. Choi, W. *et al.* Fabrics with Tunable Oleophobicity. *Adv. Mater.* **21**, 2190–2195 (2009).
24. Cheng, M. *et al.* A Functionally Integrated Device for Effective and Facile Oil Spill Cleanup. *Langmuir* **27**, 7371–7375 (2011).
25. Xue, Z. *et al.* A Novel Superhydrophilic and Underwater Superoleophobic Hydrogel-Coated Mesh for Oil/Water Separation. *Adv. Mater.* **23**, 4270–4273 (2011).
26. Yang, J. *et al.* Superhydrophilic–superoleophobic coatings. *J. Mater. Chem.* **22**, 2834–2837 (2012).
27. Deng, D. *et al.* Hydrophobic Meshes for Oil Spill Recovery Devices. *ACS Appl. Mater. Interfaces* **5**, 774–781 (2013).
28. Howarter, J. A. & Youngblood, J. P. Amphiphile grafted membranes for the separation of oil-in-water dispersions. *J. Colloid Interface Sci.* **329**, 127–132 (2009).
29. Kota, A. K., Kwon, G., Choi, W., Mabry, J. M. & Tuteja, A. Hygro-responsive membranes for effective oil–water separation. *Nat. Commun.* **3**, 1025 (2012).
30. Shi, Z. *et al.* Ultrafast Separation of Emulsified Oil/Water Mixtures by Ultrathin Free-Standing Single-Walled Carbon Nanotube Network Films. *Adv. Mater.* **25**, 2422–2427 (2013).
31. Zhang, W. *et al.* Superhydrophobic and Superoleophilic PVDF Membranes for Effective Separation of Water-in-Oil Emulsions with High Flux. *Adv. Mater.* **25**, 2071–2076 (2013).
32. Chen, P.-C. & Xu, Z.-K. Mineral-Coated Polymer Membranes with Superhydrophilicity and Underwater Superoleophobicity for Effective Oil/Water Separation. *Sci. Rep.* **3** (2013).
33. Kwon, G. *et al.* On-Demand Separation of Oil-Water Mixtures. *Adv. Mater.* **24**, 3666–3671 (2012).
34. Van de Witte, P., Dijkstra, P. J., van den Berg, J. W. A. & Feijen, J. Phase separation processes in polymer solutions in relation to membrane formation. *J. Membr. Sci.* **117**, 1–31 (1996).
35. Elimelech, M. & Phillip, W. A. The Future of Seawater Desalination: Energy, Technology, and the Environment. *Science* **333**, 712–717 (2011).
36. Smith, J. D. *et al.* Droplet mobility on lubricant-impregnated surfaces. *Soft Matter* **9**, 1772–1780 (2013).
37. Quéré, D. Non-sticking drops. *Rep. Prog. Phys.* **68**, 2495 (2005).
38. Jung, Y. C. & Bhushan, B. Wetting Behavior of Water and Oil Droplets in Three-Phase Interfaces for Hydrophobicity/philicity and Oleophobicity/philicity†. *Langmuir* **25**, 14165–14173 (2009).
39. Tuteja, A. *et al.* Designing Superoleophobic Surfaces. *Science* **318**, 1618–1622 (2007).
40. Baker, R. W. *Membrane technology.* (Wiley Online Library, 2000).
41. Drioli, E. & Giorno, L. *Comprehensive membrane science and engineering.* **1**, (Newnes, 2010).
42. Avendano-Gomez, J. R., Grossiord, J. L. & Clausse, D. Study of mass transfer in oil–water–oil multiple emulsions by differential scanning calorimetry. *J. Colloid Interface Sci.* **290**, 533–545 (2005).
43. Ping, Z. H., Nguyen, Q. T., Chen, S. M., Zhou, J. Q. & Ding, Y. D. States of water in different hydrophilic polymers — DSC and FTIR studies. *Polymer* **42**, 8461–8467 (2001).
44. Zhang, L., Zhong, Y., Cha, D. & Wang, P. A self-cleaning underwater superoleophobic mesh for oil-water separation. *Sci. Rep.* **3** (2013).

Acknowledgments

We gratefully acknowledge the support of Shell-MIT Energy Initiative. B.R.S. acknowledges support from the MITEI Fellowship. We gratefully thank Sergio Kapusta and Flavia Cassiola of Shell for many informative discussions.

Author contributions

B.R.S., M.N.H. and K.K.V. designed the experiments. M.N.H. fabricated and characterized the membranes, and B.R.S. performed the separation experiments and characterization the separation results. B.R.S., M.N.H. and K.K.V. wrote and edited the manuscript.

Additional information

Supplementary information accompanies this paper at http://www.nature.com/scientificreports

Competing financial interests: The authors declare no competing financial interests.

How to cite this article: Solomon, B.R., Hyder, M.N. & Varanasi, K.K. Separating Oil-Water Nanoemulsions using Flux-Enhanced Hierarchical Membranes. *Sci. Rep.* **4**, 5504; DOI:10.1038/srep05504 (2014).